# Multi-Sensor Fusion Approach for Cuff-Less Blood Pressure Measurement

Fen Miao, *Member, IEEE*, Zeng-Ding Liu, Ji-Kui Liu, Bo Wen, Qing-Yun He, and Ye Li, *Member, IEEE*

***Abstract*—Ambulatory blood pressure (BP) provides valuable information for cardiovascular risk assessment. The present cuff-based devices are intrusive for long-term BP monitoring, whereas cuff-less BP measurement methods based on pulse transit time or multi-parameter are inferior in robustness and reliability by using electrocardiogram (ECG) and photoplethysmogram signals. This study examined a multi-sensor fusion-based platform and algorithm for systolic BP (SBP), mean arterial pressure (MAP), and diastolic BP (DBP) estimation. The proposed multi-sensor platform was comprised of one ECG sensor and two pulse pressure wave sensors for simultaneous signal collection. After extracting 35 features from the collected signals, a weakly supervised feature selection method was proposed for dimension reduction because the reference oscillometric technique-based BP are intermittent and can be redeemed as coarse-grained labels. BP models were then established using a multi-instance regression algorithm. A total of 85 participants including 17 hypertensive and 12 hypotensive patients were enrolled. Experimental results showed that the proposed approach exhibited good accuracy for diverse population with an estimation error of 1.62 $\pm$ 7.76 mmHg for SBP, 1.53 $\pm$ 6.03 mmHg for MAP, and 1.49 $\pm$ 5.52 for DBP, which complied with the association for the advancement of medical instrumentation standards in BP estimation. Moreover, the estimation accuracy is with random daily fluctuations rather than long-term degradation through a maximum two-month follow-up period indicated good robustness performance. These results suggest that the proposed approach is with high reliability and robustness and thus provides a novel insight for cuff-less BP measurement.**

***Index Terms*—Blood pressure, multi-sensor fusion, feature selection, pulse pressure wave.**

Manuscript received September 12, 2018; revised February 6, 2019; accepted February 15, 2019. Date of publication March 15, 2019; date of current version January 6, 2020. This work was supported in part by the National Natural Science Foundation of China (61771465), in part by the Shenzhen Science and Technology Projects (JCYJ20170413161515911 and JCYJ20180703145202065), and in part by the Science and Technology Planning Project of Guangdong Province (2017B030308007). *(Corresponding author: Ye Li.)*

F. Miao, Z.-D. Liu, J.-K. Liu, B. Wen, and Q.-Y. He are with the Key Laboratory for Health Informatics of the Chinese Academy of Sciences, Shenzhen Institutes of Advanced Technology, Shenzhen 518055, China (e-mail: fen.miao@siat.ac.cn; zd.liu@siat.ac.cn; jk.liu@siat.ac.cn; bo.wen@siat.ac.cn; qy.he@siat.ac.cn).

Y. Li is with the Joint Engineering Research Center for Health Big Data Intelligent Analysis Technology, Shenzhen Institutes of Advanced Technology, Chinese Academy of Sciences, Shenzhen 518055, China (e-mail: ye.li@siat.ac.cn).

Digital Object Identifier 10.1109/JBHI.2019.2901724

## Abbreviations

| | |
|---|---|
| BP | Blood pressure |
| PTT | Pulse transit time |
| ECG | Electrocardiogram |
| PPG | Photoplethysmogram |
| SBP | Systolic BP |
| MAP | Mean arterial pressure |
| DBP | Diastolic BP |
| PPW | Pulse pressure waveform |
| ICG | Impedance cardiogram |
| MIMICII | Multi-parameter Intelligent Monitoring in Intensive Care II |
| AAMI | Association for the Advancement of Medical Instrumentation |
| ICU | Intensive care unit |
| PWV | Pulse wave velocity |
| M-K | Moens–Korteweg |
| PPWr | Radial artery PPW |
| PPWa | Ankle artery PPW |
| WSF | Weakly supervised feature selection |
| ME | Mean error |
| STD | Standard deviation of the error |
| MAE | Mean absolute error |
| CP | Cumulative percentage |
| BHS | British Hypertension Society |
| MCFS | Multi-cluster feature selection |
| USF | Unsupervised spectral feature selection |

## I. Introduction

GLOBAL hypertension prevalence is high and rising in both developed and developing countries. Long-term hypertension can result in various complications such as coronary heart disease, stroke, and heart failure [1], [2]. However, awareness of the risk of hypertension is low, and individuals with hypertension rarely seek treatment; consequently, it is known as the "silent killer" [3]. According to a recent large-cohort study in China, awareness and treatment rates of hypertension was only 36% and 22.9%, respectively [4]. Although blood pressure (BP) can be accurately measured through invasive methods, such measurement is impractical in daily life because it requires insertion of a catheter, which means that professional intervention is necessary; moreover, the procedure causes severe pain. Today, noninvasive BP measurement relies on inflation with a cuff, including the auscultation method and oscillometric technique, and these are the most common methods for routine examination

of BP at clinics. However, cuff-based methods are inconvenient, intrusive for long-term BP measurement. An unobtrusive device for long-term BP monitoring would help improve awareness regarding the risks of hypertension, thereby helping to reduce the incidence of cardiovascular disease [5].

Recently, several approaches have been proposed for cuff-less BP measurement, including oscillometric finger pressing based [6], [7], ultrasound based [8], [9], pulse transit time (PTT) based [10]–[18] and multi-parameter based approaches [19]–[26]. In 2018, Chandrasekhar *et al.* firstly proposed an oscillometric finger-pressing method for BP monitoring that can deployed on smartphone platform [6], and then developed an iPhone application with an accuracy of $-4.0 \pm 11.4$ mmHg for systolic BP (SBP) and $-9.4 \pm 9.7$ mmHg for diastolic BP (DBP) [7]. Ultrasound-based method was also developed for continuous BP measurement and showed promising results but with higher complexity [8], [9]. PTT based approaches have been studied extensively over several years and always been the most popular methods for cuff-less BP measurement [10]–[18]. As a potential indicator for BP, PTT refers to the time for a pulse wave to travel between two locations in the cardiovascular system [10]. PTT can be calculated from two pulse signals generated by the cardiovascular system, such as electrocardiogram (ECG) and photoplethysmogram (PPG) signal, two-channel PPG, or impedance cardiogram (ICG) and PPG [11]–[13]. A novel approach for obtaining PTT from ballistocardiogram (BCG) and PPG monitoring at the ear [26] was also proposed by He *et al.*, which provided a novel insight to monitor BP in a wearable way. Based on the potential relationship between PTT and BP, various models have been proposed for BP estimation, such as nonlinear model by Poon *et al.* [14] and model combining PPG intensity ratio and PPT [17]. However, because of the fixed relationship hypothesis, PTT-based models are marred by low accuracy and robustness, meaning that frequent calibrations are required to ensure estimation accuracy [18] because other factors such as vascular tone, physiological status and individual variability affect the relationship between PTT and BP. Lin *et al.* demonstrated that the addition of PPG indicators of vascular tone can improve the accuracy of PTT based models [19]. Consequently, more multi-parameter based approaches have been studied by merging various parameters that influence BP [20]–[25]. Numerous features have been extracted from ECG and PPG signals in these studies and used to construct BP models using machine learning algorithms. In [20], physiological parameters and whole-based representation of ECG and PPG signals were extracted to estimate BP through supervised machine learning regression models. Experimental results based on the public Multi-parameter Intelligent Monitoring in Intensive Care II (MIMICII) waveform database showed that the proposed method complied with the Association for the Advancement of Medical Instrumentation (AAMI) standards for mean arterial pressure (MAP) and diastolic BP (DBP) estimation. Miao *et al.* also verified the performance of multi-parameter based BP models using data mining techniques; the results showed that this type of method outperformed PTT based methods in estimation accuracy [22].

However, most of PTT and multi-parameter based BP models were verified on young healthy populations and thus with low reliability while applied to diverse population, while others on intensive care unit (ICU) patients used the public MIMICII database are weak in detailed experimental protocols and validation for routine examination. In another aspect, robustness must be improved because of the degradation to performance seen after 1 day. Possible reasons for this degradation include, the indistinctive pulse characteristic in PPG signals due to the influence of peripheral microvascular tissue resistance smoothing the PPG morphology [27]; as well as high-sensitivity in PTT calculated from ECG and finger PPG. The pulse pressure waveform (PPW), which is rich in significant characteristic information such as dicrotic wave for diverse population, has been well-studied for evaluation of arterial stiffness and cardiac function [28], [29]. However, few studies exist regarding the utility of the PPW for cuff-less BP estimation. Today, the PPW can be collected in a wearable and stable manner because of the development of electric fabrics and flexible pressure sensors [30], [31], which can further strengthen the feasibility of using the PPW for cuff-less and wearable BP estimation. Moreover, the combination of multiple sensors to calculate different measures of PTT has the potential to discover that with highest stabilization and thus improve the robustness of PTT and multi-parameter based models.

This study examined a novel concept for BP estimation based on a multi-sensor platform comprising one-channel ECG and two-channel PPW signals. To our best knowledge, this is the first comprehensive study taking advantage of multi-sensor fusion technique, diverse population and long-term follow-up to make several contributions to the field of BP measurement. First, different measures of PTT and various features extracted from PPW signals were evaluated in BP estimation, with an emphasis on a feature fusion to provide an accurate and robust model. Second, the performance was validated by an elaborated designed experimental protocol involving a large number of participants (including hypertensive patients and hypotensive patients) and followed up for a maximum of 2 months, and thus indicated the reliability of our study. Finally, to resolve the weakly supervised problem inherent to intermittent cuff-based BP as the reference, a weakly supervised feature selection method was proposed based on spectral analysis for dimension reduction.

The rest of the paper is organized as follows. After presenting the principal of PPW measurement in Section II, the multi-sensor platform and experimental protocol is introduced in Section III. The proposed methodology is described in Section IV. Experimental results are provided in Section V, and a discussion on the implications of the proposed approach is presented in Section VI. Section VII concludes the paper.

## II. Background

BP is produced by blood flow through the arterial vessels, which are similar to elastic tubes. Several factors are responsible for BP fluctuations, including vessel elasticity, peripheral resistance, cardiac output, and blood volume [32]. In this section, we provide a brief discussion of the principal of PPW measurement and theory regarding the factors extracted from ECG and PPW signals that can influence BP.

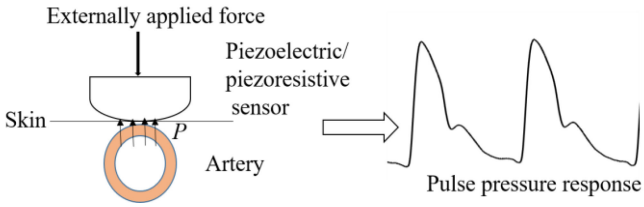


Fig. 1. Principal of pulse pressure wave measurement.

### A. Principles of PPW Measurement

The pulse wave, which comes directly from the heart into the blood vessel system, is one of the most critical signs of human life. Pulse wave analysis based on pulse contour and pulse characteristics can be used to evaluate blood vessel function in terms of cardiac output and conditions such as hypertension and arterial stiffness [33]–[35].

Two common technologies to measure pulse wave including photoplethysmography (i.e., PPG signal) and pressure sensing (i.e., PPW signal). PPG signals are detected based on photoelectric inspection technique to reflect the volume change in capillary, while PPW signals are detected from superficial artery via piezoelectric or piezoresistive effect to reflect the dynamic pressure change during each pulse cycle. Compared with PPG, PPW is an intuitive representative of pressure and with significant characteristic information [36]. Fig. 1 depicts the principal of PPW measurement. A piezoelectric or piezoresistive sensor is applied to the skin overlying the artery. The PPW can be detected by transforming the pulse pressure on the sensor (denoted as *P* in Fig. 1) to electrical signal due to the change in artery diameter during each pulse cycle while an externally applied force is applied. It is different from arterial tonometry, in which the artery should be partially flattened or applanated to reflect intraluminal pressure; however, applanation has demonstrated to be difficulty and thus frequent calibration is needed in arterial tonometry technique [37].

### B. Relationship Between PTT and BP

Vessel elasticity is one of the most important factors influencing BP fluctuations. Hughes *et al.* [38] noted that vascular elasticity $E$ is related to the pressure $P$ as

$$E = E_0 e^{\alpha P} \tag{1}$$

Where $P$ is mean BP, $E_0$ is a subject-dependent parameter that denotes the vascular elasticity when the pressure is 0, and $\alpha$ is the correction factor.

The pulse wave velocity (PWV) is the velocity at which the arterial pulse propagates through the vascular system. From the Moens–Korteweg (M–K) equation [39], the PWV is directly related to the arterial wall stiffness as follows:

$$PWV = \sqrt{\frac{Eh}{2r\rho}} \tag{2}$$

Where $\rho$ is the blood density, $r$ is the vessel radius, and $h$ is the vessel wall thickness. The M–K equation indicates that, given constant $\rho$, $h$, and $r$, PWV is proportional to the square root of vascular elasticity. Combining (1) and (2), we can obtain

$$PWV = \sqrt{\frac{E_0 e^{\alpha P} h}{2r\rho}} \tag{3}$$

Which indicates that PWV has a positive correlation with mean BP.

An alternative method for measuring PWV is utilizing the feature points of the arterial waveforms measured from two sites to calculate the time interval, that is, PTT, from the following formula:

$$PTT = L/PWV \tag{4}$$

Where $L$ is the distance between the two sites from which the arterial waveforms were collected. PTT can be measured from the specific feature points in various pulse waves (i.e., ECG, PPG, and ICG) [11], [40]. The most common measure is the time delay between an ECG R peak and the maximum of the first derivative of PPG. However, this measurement of PTT remains controversial because of the inclusion of the pre-ejection period (PEP) [41], [42]. In this study, three measures of PPT were calculated from three sensors and evaluated for BP estimation: PTT from ECG to the radial artery PPW (PPWr), PTT from ECG to the ankle artery PPW (PPWa), and PTT from PPWr to PPWa.

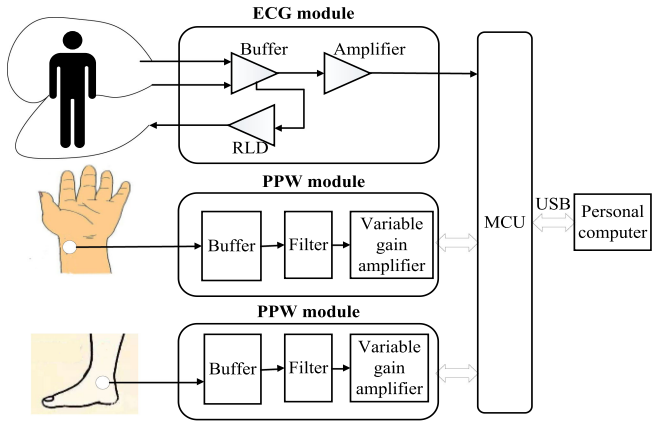


Fig. 2. Block diagram of the multi-sensor platform.

## III. Multi-Sensor Platform and Experimental Protocol

### A. The Multi-Sensor Platform

The block diagram of the multi-sensor platform is presented in Fig. 2. The multi-sensor platform is comprised of one ECG module and two PPW modules for simultaneous signals collection. The detail information of the PPW module (HK-2000B, Hefei Huake Electronic Technology Research Institute, Hefei, China) was described in our previous work [43]. The acquired signals were converted to digital signal by an analog-to-digital converter inside the microcontroller unit (denoted as MCU in

Fig. 3. Experimental scenario.

Fig. 2). Then, the digital signal was sent to the personal computer for real-time display via USB port.

### B. Experimental Protocol

A total of 85 participants (33 men and 52 women) with a mean age of 49.94 ± 9.01 years were recruited for our study. Among them, 17 participants are hypertensive patients (mean SBP greater than 140 mmHg or mean DBP greater than 90 mmHg over three measurements of BP using the oscillometric technique), and 12 participants are hypotensive patients (mean SBP less than 90 mmHg or mean DBP less than 60 mmHg over three measurements of BP). None of them had taken antihypertensive drugs before the study was conducted. Fig. 3 illustrates the experimental scenario. Each participant was required to lie down quietly for 5 minutes before the measurement and during data collection to avoid interference caused by emotional and physiological changes, and motion artifacts. The reference SBP and DBP were measured using a cuff-based BP device (OMRON HEM-7200, OMRON Industrial Automation, Japan) worn on the right upper arm. Simultaneously, 1-minute ECG and two-channel PPW were continuously and simultaneously acquired using the multi-sensor platform during BP measurement. ECG signals were collected in detail through ECG electrodes placed on the left and right arms and right leg; two-channel PPW was collected separately from the radial artery located in the left wrist and ankle artery located in the left ankle. The sampling frequency for ECG and the PPW was set to 2500 Hz.

The experimental procedure consisted of two sessions: a training session (calibration session) and a validation session, which are presented in Fig. 4. Fig. 4(A) and Fig. 4(B) presents the experimental protocol and overall BP data points collected from all the 85 participants, separately. In the training session, a total of 16 measurements evenly distributed between 9 a.m. and 6 p.m. on the first day (D) were collected to form the training dataset for each subject. Another 16 measurements with 4 measurements distributed at a random time slot on D+1, D+3, D+6, and D+8, separately, were collected to form the test dataset for each subject. Ten participants were randomly selected for data collection on D+60 to verify long-term performance. Herein D+1, D+3, D+6, D+8 and D+60 means 1 day, 3 days, 6 days, 8 days and 60 days after the calibration session (D), separately. For each measurement, reference SBP and DBP, 1-minute ECG

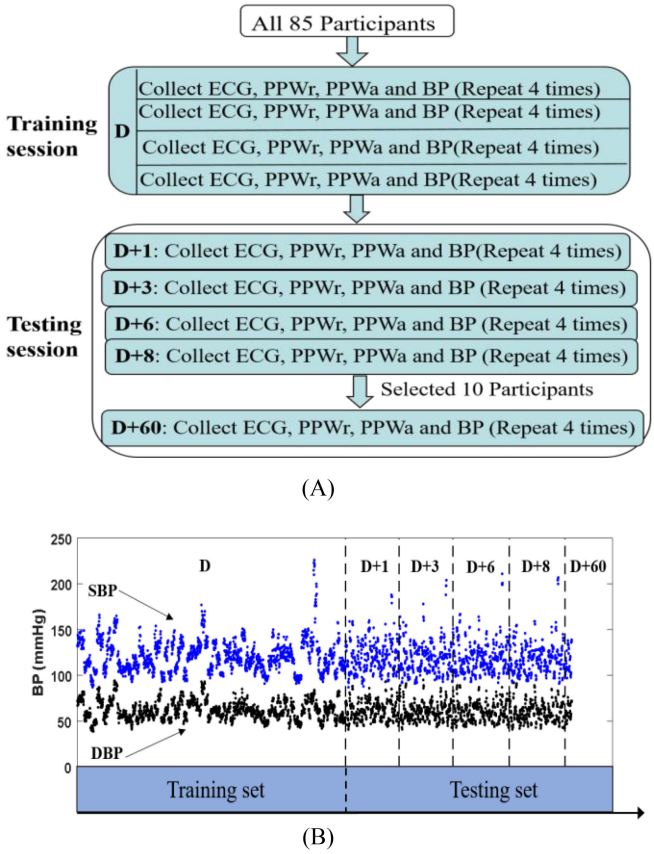


Fig. 4. Experimental procedures at D, D+1, D+3, D+6, D+8, and D+60. (A) Experimental protocol. (B) Collected BP data.

and two-channel PPW were collected through their respective methods. For each subject, the training dataset collected on day D was employed to establish an individual BP model, and the independent test dataset collected on the following days was employed to verify the estimation accuracy and robustness of the proposed model.

This study was approved by the Institutional Ethics Committee of the Shenzhen Institute of Advanced Technology, Chinese Academy of Sciences. We obtained informed consent from all participants before the experiment.

The collected database consisted of 2720 measurements with a mean SBP of 120.91 ± 17.84 mmHg and DBP of 72.15 ± 10.36 mmHg. The statistical information regarding the distribution of the SBP and DBP is presented in Fig. 5(A). Fig. 5(B) presents the distribution of dynamic range in SBP and DBP for individuals, suggesting that BP is significantly changed during the process with a mean dynamic range of 26 mmHg for SBP and 18 mmHg for DBP.

## IV. Methodology

Fig. 6 illustrates the block diagram of the proposed BP estimation approach via multi-sensor fusion, which is comprised of the following steps: 1) collect three-channel signals, including ECG, PPWr and PPWa from a multi-sensor platform, as the inputs of the approach; 2) extract the features from the collected

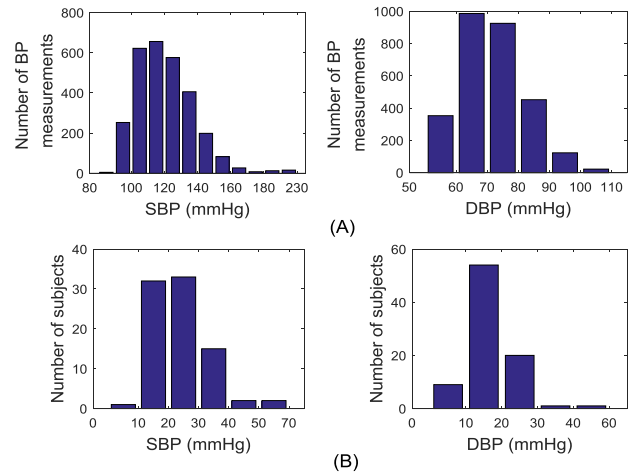


Fig. 5. SBP and DBP. (A) Statistical distribution of BP measurements. (B) Individual BP dynamic range distribution.

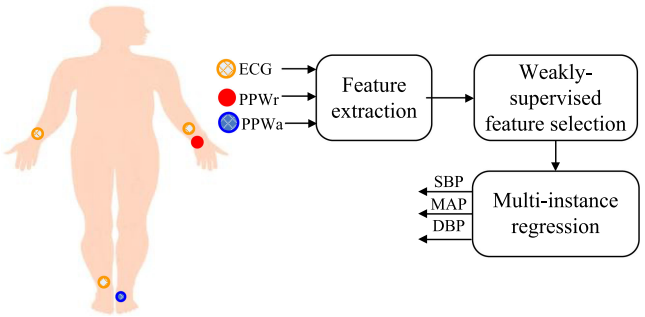


Fig. 6. Block diagram of the proposed BP estimation approach. PPWr: PPW signals collected from the radial artery; PPWa: PPW signals collected from the ankle artery.

signals, including physiological parameters and informative parameters; 3) select the crucial feature by a weakly-supervised feature selection method; 4) develop the models for SBP, MAP and DBP via multi-instance regression algorithm.

### A. Feature Extraction

Two types of features can be extracted from each beat of ECG and PPW signal: physiological parameters and informative parameters. Physiological parameters are calculated from the feature points with physical significance (e.g., PTT and systolic time), whereas informative parameters are the whole informative representation of the signal properties (e.g., low- and high-power frequency of the signal).

*1) Extraction of Physiological Parameters:* These features include the time shift between specific feature points of the ECG and two-channel PPW signals (different measures of PTT) and the shape parameters of the PPW signal inspired from physical significance. The detailed definitions of the extracted physiological parameters are presented as follows: 24 (numbered from 1 to 24 and listed in Table I) physiological features were calculated from the ECG and two-channel PPW signals, as shown in

TABLE I
DEFINITIONS OF EXTRACTED PHYSIOLOGICAL AND INFORMATIVE PARAMETERS

| Features | Definitions | Equations |
|---|---|---|
| (1) PTTeb | Time span between the ECG R peak and the maximum of first dPPWr | PTTeb |
| (2) PTTea | Time span between the ECG R peak and the maximum of first dPPWa | PTTea |
| (3) PTTba | Time span between the maximum of first dPPWr and first dPPWa | PTTba |
| (4) RtAmCE | Amplitude ratio of point C and point E | P2/P1 |
| (5) TmAE | Time span between point A and point E | T2 |
| (6) TmBE | Time span between point B and point E | T3 |
| (7) TmCD | Time span between point C and point D | T4 |
| (8) RtTP | Time ratio of T4 to peak interval | T4/T1 |
| (9) K | PPWr characteristic value | Formula (10) |
| (10) K1 | Systolic characteristic value | Formula (11) |
| (11) K2 | Diastolic characteristic value | Formula (12) |
| (12) AS | Ascending slope of PPWr | $\sum_{i=A}^{C}(P_i - P_A)$ |
| (13) first dPPW_PAm | Peak Amplitude of first dPPWr | P3 |
| (14) first dPPW_TW | Time width of first dPPWr | T6 |
| (15) second dPPW_TAm | Total Amplitude of second dPPWr | P5 |
| (16) second dPPW_PAm | Peak Amplitude of second dPPWr | P6 |
| (17) second dPPW_FAm | Foot Amplitude of second dPPWr | P7 |
| (18) first dPPW_AS | Ascending slope of first dPPWr | P3/T5 |
| (19) first dPPW_DS | Descending slope of first dPPWr | P4/T6 |
| (20) first dPPW_AA | Ascending area of first dPPWr | $\sum_{i=F}^{C}(P_i^{'} - P_F^{'})$ |
| (21) second dPPW_AS | Ascending slope of second dPPWr | P6/T7 |
| (22) second dPPW_DS | Descending slope of second dPPWr | P5/T8 |
| (23) second dPPW_AA | Ascending area of second dPPWr | $\sum_{i=N}^{M}(P_i^{*} - P_N^{*})$ |
| (24) PIR | Ratio of PPWr peak to foot amplitude | PL/PH |
| (25) MN | Average value of the signal | $\sum_{i=1}^{n}\frac{ppw_i}{n}$ |
| (26) SD | Standard deviation of a signal | $\sum_{i=1}^{n}\frac{(ppw_i - mn)^2}{n}$ |
| (27) Skewness | Steep slow degree | Formula (13) |
| (28) Kurtosis | the degree of peakedness of the distribution | Formula (14) |
| (29) Fre1 | Amplitude at fundamental frequency | F1in Fig. 9 |
| (30) Fre2 | Amplitude at the 1st harmonics | F2 in Fig. 9 |
| (31) Fre3 | Amplitude at the 2nd harmonics | F3 in Fig. 9 |
| (32) Fre4 | Amplitude at the 3rd harmonics | F4 in Fig. 9 |
| (33) Approximate entropy | Unpredictability of fluctuations for signal | Formula (15) |
| (34) Sample entropy | Unpredictability of fluctuations for signal | Formula (16) |
| (35) Wavelet energy entropy | Complexity of the signal | Formula (20) |

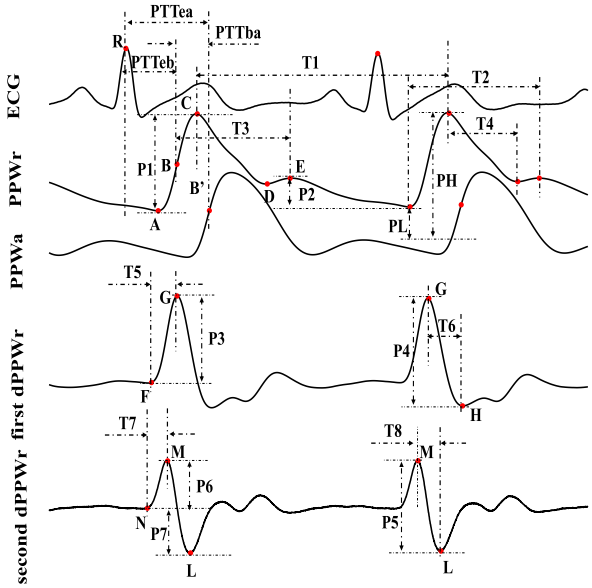


Fig. 7. Extracted physiological features.

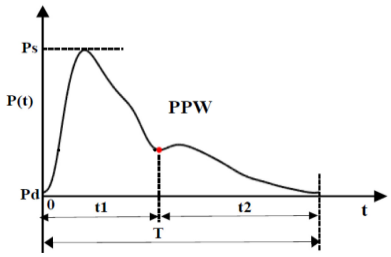


Fig. 8. Definition of *K* value in PPW.

Figs. 7 and 8. Detailed interpretation and calculation methods for the extracted features are presented in Table I.

Fig. 7 illustrates the extracted features. In Fig. 7 and Table I, the letters A, C, D, and E represent the foot, peak, foot of the dicrotic wave, and peak of the dicrotic wave in the PPWr, respectively; the letters F, G, and H represent the start, peak, and foot, respectively, in the first derivate of the PPWr signal (first dPPWr); and the letters N, M, and L represent the start, peak, and foot, respectively, in the second derivate of the PPWr signal (second dPPWr). Point B and B′ are the maximum point of the first dPPWr and the first derivate of the PPWa signals (first dPPWa), respectively. PTT was calculated as the time interval from the ECG R peak to the peak of the first dPPW in the same cardiac cycle. The three *K* values are presented in Fig. 8 and were calculated using the following formula:

$$K = \frac{P_m - P_d}{P_s - P_d} \tag{5}$$

$$K_1 = \frac{P_{m1} - P_d}{P_s - P_d} \tag{6}$$

$$K_2 = \frac{P_{m2} - P_d}{P_s - P_d} \tag{7}$$

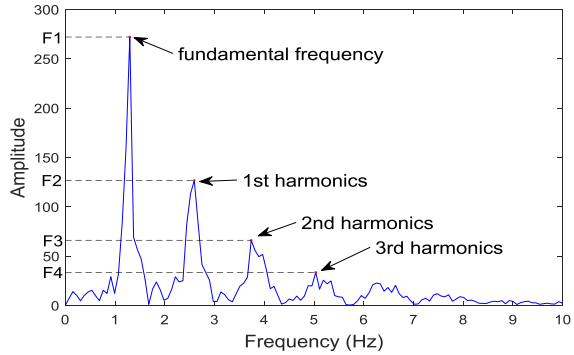


Fig. 9. Definition of features in the frequency domain.

Where $P_m = \frac{1}{T}\int_0^T P(t)$, $P_{m1} = \frac{1}{t1}\int_0^{t1} P(t)$, $P_{m2} = \frac{1}{t2}\int_{t1}^{t1+t2} P(t)$.

*2) Extraction of Informative Parameters:* These features are whole representations of signal properties that have no clear physical significance. In this paper, 11 features (numbered from 25 to 35 in Table I) based on time and frequency domain, information theory, and wavelet domain were extracted from PPWr signals. Given a PPWr sequence within a pulse cycle $PPW = \{ppw_1, ppw_2, \ldots, ppw_n\}$, the computation method for each index is as follows.

*a) Time Domain:* Four features were extracted from time domain; mean, standard deviation, skewness, and kurtosis (Table I); in which the skewness and kurtosis can be calculated as (8) and (9), respectively.

$$Skewness = \frac{n}{(n-1)(n-2)} \sum_{i=1}^{n} (ppw_i - MN)^3 / SD^3 \tag{8}$$

$$Kurtosis = \frac{n(n+1)\sum (ppw_i - MN)^4 - 3\left(\sum (ppw_i - MN)^2\right)^2 (n-1)}{(n-1)(n-2)(n-3)SD^4} \tag{9}$$

Where *MN* and *SD* are the mean and standard derivation of the signal *PPW*.

*b) Frequency Domain:* Four features were extracted from frequency domain. Fig. 9 presents an example of the Fourier transformation of the PPWr signal; we extracted the four features as the amplitude at fundamental frequency and the following three harmonics, which can detected from the first four maximum-frequency amplitudes.

*c) Entropy Properties:* Entropy describes the confusion degree of a system; greater entropy means higher confusion [44]. Two common indices, approximate entropy and sample entropy, are features of entropy theory. The approximate entropy and sample entropy for time series data can be calculated as follows.

For a time series of data $u(1), u(2), \ldots, u(N)$, fix the length of compared run of data $m$ and filtering level $r$. Then, form a sequence of vectors $\mathrm{x}(1), \mathrm{x}(2), \ldots, \mathrm{x}(\mathrm{N}-\mathrm{m}+1)$, where $\mathrm{x}(i) = [u(i), u(i+1), \ldots, u(i+m-1)]$. For each $i, 1 \le i \le N-m+1$, construct $C_i^m(r) = (number\ of\ x(j)$

*such that* $d[x(i), x(j) \leq r]/(N-m+1)$, in which $d[x, x^*] = \max|u(a) - u^*(a)|$.

Define $\Phi^m(r) = (N-m+1)^{-1}\sum_{i=1}^{N-m+1}\log(C_i^m(r))$ and $B^m(r) = (N-m+1)^{-1}\sum_{i=1}^{N-m+1}C_i^m(r)$; approximate entropy can be calculated as

$$ApEn = \Phi^m(r) - \Phi^{m+1}(r) \tag{10}$$

Sample entropy can be calculated as

$$SampEn(m, r, N) = -\log(B^{m+1}(r)/B^m(r)) \tag{11}$$

*d) Wavelet Domain:* The wavelet energy entropy can provide quantitative information regarding the complexity of signals, and it has been used for arterial stiffness analysis [45]. To calculate the wavelet energy entropy, the wavelet coefficients $c_j$ were first obtained at each resolution level $j$. The energy at scale $j = 1, 2, \ldots J$ is defined as

$$E_j = \sum_{j}^{J}|c_j(k)|^2 \tag{12}$$

Where $c_j(k)$ is the coefficient at time $k$ at level $j$, and the total energy is

$$E_{tol} = \sum_{j}^{J}\sum_{k}^{N}|c_j(k)|^2 = \sum_{j}E_j \tag{13}$$

The relative wavelet energy, which defines the energy's probability distribution in scales, is given by

$$p_j = \frac{E_j}{E_{tol}} \tag{14}$$

Thus $\sum_j p_j = 1$. The wavelet energy entropy is, in turn, defined as

$$H_{WT}(p) = -\sum_{j}^{J}p_j \cdot \ln(p_j). \tag{15}$$

In this study, the PPWr was decomposed to five decomposition levels with a coiflet3 mother wavelet, and the wavelet energy entropy was subsequently calculated from wavelet coefficients.

## B. Weakly Supervised Feature Selection Through Spectral Analysis

The extracted features presented in the previous section were highly correlated, and thus a feature selection method was required to improve the training efficiency. Existing feature selection methods include supervised and unsupervised methods. However, as presented in the experimental procedure, cuff-based BP providing intermittent collection through the oscillometric method was used as the reference; during each BP collection interval, 1-minute continuous physiological signals were collected. Accordingly, as in Fig. 10, one pair of BP values corresponded to a batch of feature sets extracted from each heartbeat. For this question, the task was to learn $f : X \mapsto \mathrm{Y}$ from a training dataset $T = \{(X_1, y_1), \ldots, (X_m, y_m)\}$ , where $X_i = \{\mathbf{x}_{i1}, \ldots, \mathbf{x}_{im_i}\} \subseteq \mathrm{X}$ is called a bag, and $m_i$ is the number of instances in the $i_{th}$ bag; $y_i \subseteq \mathrm{Y}$ is the label for the $i_{th}$ bag. We aimed to predict labels for unseen bags. Thus, it is a weakly supervised question or multi-instance question because only coarse-grained label information is available [46].

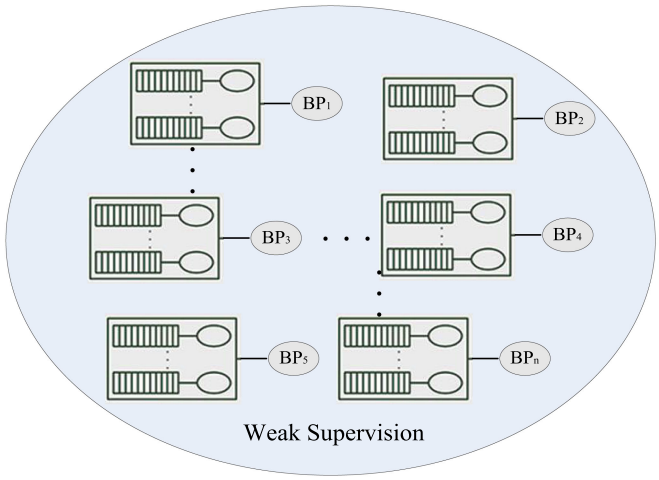


Fig. 10. Illustration of the weakly supervised scenario for BP estimation.

Spectral analysis can be employed in supervised and unsupervised feature selection, demonstrating favorable performance [47], [48]. Herein, we propose a weakly supervised feature (WSF) selection method to select the most important features for BP model development based on spectral analysis.

*1) Similarity Assessment:* Suppose we have dataset $D$ and bag label Y, for each instance $\mathbf{x}_i$ in $D$, the corresponding label is initialized as the bag label $y_i = Y_I$ for $i \in I$. The dissimilarity between each pair of instances can be measured by the distance between them. A good measure of distance to reflect instance similarity is critical in feature selection. In this study, we first defined four constraint sets that represented the distance level between each pair of instances based on their weak labels, which are denoted as $M_1$ if $|y_i - y_j| \leq 5$, $M_2$ if $5 < |y_i - y_j| \leq 10$, $M_3$ if $10 < |y_i - y_j| \leq 15$, and $M_4$ if $|y_i - y_j| > 15$. In this case, instances belonging to the same bag are attributed to $\mathrm{M}_1$ constraints. According to the geometric structure of the data and different constraint sets, a set of pairwise instances with similarity $\mathbf{S} = \{S_{ij}\}$ $i, j = 1, 2, \ldots n$ can be constructed to represent the relationships among different instances, which can be defined as follows:

$$S_{i,j} = S_{j,i} = \begin{cases} \omega_1 e^{\frac{-\|x_i - x_j\|^2}{2\sigma^2}}, & \text{if } \mathrm{x_i} \in \mathrm{M_1\ (x_j)\ and\ x_j} \in \mathrm{M_1\ (x_i)} \\ \omega_2 e^{\frac{-\|x_i - x_j\|^2}{2\sigma^2}}, & \text{if } \mathrm{x_i} \in \mathrm{M_2\ (x_j)\ and\ x_j} \in \mathrm{M_2\ (x_i)} \\ \omega_3 e^{\frac{-\|x_i - x_j\|^2}{2\sigma^2}}, & \text{if } \mathrm{x_i} \in \mathrm{M_3\ (x_j)\ and\ x_j} \in \mathrm{M_3\ (x_i)} \\ 0, & \text{otherwise} \end{cases} \tag{16}$$

Where $\omega_1 > \omega_2 > \omega_3 > 0$ are the reward values for similar constraints.

*2) Feature Selection Based on Spectral Analysis:* Given an instance set X, we use $\mathbf{G}(V, E)$ to denote the undirected graph constructed from $\mathbf{S}$, where $V$ is the vertex set and $E$ is the

TABLE II
MULTI-INSTANCE REGRESSION ALGORITHM

| *Multi-instance regression algorithm* |
|---|
| **Input** = dataset $D$ and bag label $Y$<br>**Output** = regression function $f$<br>1. For each instance $\mathrm{x}_i$ in $D$, initialize the corresponding label as the bag label $y_i = Y_I$ for $i \in I$. The sample set is initialized as $U = \{\mathrm{x}_i, y_i\}$ for $\mathrm{x}_i \in D$. |
| 2. REPEAT.<br>3. Train a regression function $f$ with all the samples in $U$ with imputed labels.<br>4. Predict the label for each instance with $f$.<br>5. Empty U.<br>6. Choose the samples with the lower prediction error to form U to eliminate instances with high derivation.<br>7. UNTIL (prediction error is less than 15 mmHg).<br>8. Return $f$. |

edge set. The $i_{th}$ vertex $v_i$ of $G$ corresponds to $\mathbf{x}_i$, and there is an edge between each vertex pair $(v_i, v_j)$ where the weight is determined by $\mathbf{S}$; that is, $w_{ij} = S_{ij}$. Given $G$, its adjacency matrix $W$ is defined as $W(i,j) = w_{ij}$. The degree matrix $D$ of the graph $G$ is defined by

$$D(i,j) = \begin{cases} \sum_{k=1}^{n} w_{ik}, & \text{if } i = j \\ 0, & \text{otherwise} \end{cases}. \tag{17}$$

Given the adjacent matrix and degree matrix $D$, the Laplacian Matrix $L$ and the normalized Laplacian Matrix can be defined as

$$L = D - W; \mathcal{L} = D^{-\frac{1}{2}} L D^{-\frac{1}{2}}. \tag{18}$$

We then calculate the spectral decomposition $(\lambda_i, \xi_i)$ of the normalized Laplacian matrix, where $\lambda_i$ is the eigenvalue and $\xi_i$ is the eigenvector $(0 \le i \le n-1)$. Assuming $\lambda_0 \le \lambda_1 \le \cdots \le \lambda_{n-1}$, according to spectral clustering theories, $\lambda_i (0 \le i \le n-1)$ measures the separability of the components of the graph and the corresponding soft cluster indicators. Therefore, we sort the top $p$ ranked features $\{\xi_1, \xi_2, \ldots, \xi_p\}$ corresponding to the first $p$ maximum eigenvalues as the selected features.

### C. Model Development and Validation

For the weakly supervised regression task, a multi-instance regression algorithm was proposed. This algorithm trains a regression function through an alternative optimization process including a supervised regression and label updating process, which is detailed in Table II.

We evaluated the agreement between the BP values estimated by the proposed model and reference BP values on the test dataset. Mean error (ME), standard deviation of the error (STD), and mean absolute error (MAE) between estimated BP with the proposed approach and reference BP were used as the evaluation metrics. The agreement between estimated and reference BP were analyzed in terms of the following scores. First, correlation and Bland–Altman analysis was performed to verify the consistency between the model and reference. Furthermore, two most widely used standards for evaluating the accuracy of BP devices, including British Hypertension Society standard (BHS) [49] and AAMI standard [50], were used to verify the performance of the proposed approach. As a standard firstly published by British Hypertension Society in 1990, the BHS standard grades BP measurement devices based on the cumulative percentage of estimated BP computed by the proposed model falling within the reference BP values of $\pm 5$, $\pm 10$, and $\pm 15$ mmHg. While AAMI standard, which was approved in 2002 by American National Standards Institute, requires difference between the proposed model and the reference with mean and standard value lower than 5 and 8 mmHg. We also evaluated the estimation accuracy at different calibration intervals to verify the robustness of the proposed model.

TABLE III
PERFORMANCE COMPARISON BETWEEN THE PROPOSED WSF AND BASELINE FEATURE SELECTION ALGORITHMS

| Algorithm | Average MAE | Average redundancy rate |
|---|---|---|
| **WSF** | **6.56** | **0.193** |
| USF[42] | 6.66 | 0.222 |
| ReliefF[46] | 6.70 | 0.207 |
| MCFS[47] | 6.90 | 0.296 |

## V. EXPERIMENTAL RESULTS

### A. Feature Selection Results

To verify the performance of the proposed WSF approach, three representative feature selection methods, ReliefF [51], multi-cluster feature selection (MCFS) [52] and unsupervised spectral feature selection (USF) [41], were chosen for comparison. A common hypothesis for evaluating the quality of a feature subset is that if a feature subset is more relevant to the target, learning should achieve lower estimation error. Smaller correlation between each feature also indicates higher quality. Therefore, we compared the estimation error in terms of MAE and redundancy rate of the proposed feature selection method and baseline methods.

Assume $F$ is the selected feature set, and the redundancy rate is measured by

$$RED(\mathrm{F}) = \frac{1}{m(m-1)} \sum_{f_i, f_j \in \mathrm{F}, i>j} \rho_{i,j}, \tag{19}$$

Where $\rho_{i,j}$ is the correlation between the $i$-th and the $j$-th feature, and $m$ is the number of features in the selected feature set.

The MAE versus different numbers of selected features with SBP as the example is shown in Fig. 11. As illustrated in the figure, the proposed WSF is with consistent lower MAE than the other three feature selection algorithms. Table III shows the average MAE and redundancy rate for different numbers of selected features. WSF outperforms baseline algorithms with a maximum decrease of 0.34 in average MAE and decrease of 0.1 in average redundancy rate. This observation suggests

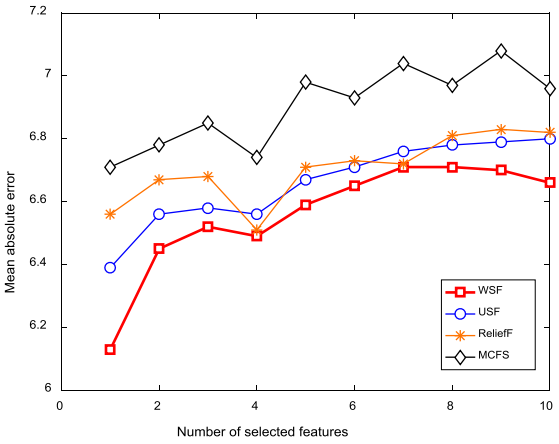


Fig. 11. Estimation error vs. different numbers of selected features. Lower prediction error is preferred.

TABLE IV
TOP 15 IMPORTANT FEATURES CONTRIBUTE TO THE FINAL FEATURE SET

| Features | SBP | DBP |
|---|---|---|
| (1)PTTea | 0.115 | 0.098 |
| (24)PIR | 0.104 | 0.117 |
| (26)SD | 0.092 | 0.089 |
| (5)TmAE | 0.081 | 0.063 |
| (6)TmBE | 0.075 | 0.097 |
| (21)second dPPW_AS | 0.073 | 0.073 |
| (29) Fre1 | 0.071 | 0.065 |
| (22)second dPPW_AA | 0.061 | 0.059 |
| (23)second dPPW_DS | 0.049 | 0.075 |
| (30)Fre3 | 0.041 | 0.046 |
| (11)K2 | 0.039 | 0.052 |
| (27)Skewness | 0.031 | 0.023 |
| (9)K | 0.026 | 0.031 |
| (14)first dPPW_TW | 0.024 | 0.022 |
| (12) Approximate entropy | 0.019 | 0.015 |

that the proposed WSF outperforms existing algorithms for BP estimation.

We further evaluate the importance of each variable presented in Table I by computing their contribution ratio to the final selected features. Assume, the final feature sets as $\mathbf{F} = \{\mathrm{F}_1, \mathrm{F}_2, \ldots, \mathrm{F}_N\}$, where $N$ is the number of features selected; the original feature set as $\mathbf{f} = \{\mathrm{f}_1, \mathrm{f}_2, \ldots, \mathrm{f}_M\}$, where $M$ is the number of original features. The transformation between f and F can be described as: $\mathbf{F} = \mathbf{A}\mathbf{f}$, where $\mathbf{A} = \{a_{ij}\}$ $i = 1, 2, \ldots, M$ and $j = 1, 2, \ldots, N$. The contribution ratio for variable $\mathrm{f}_j$ to final feature sets can be computed as:

$$con_j = \sum_{i=1}^{N} |a_{ij}| \Big/ \sum_{j=1}^{M} \sum_{i=1}^{N} |a_{ij}| \tag{20}$$

Table IV presents the top 15 important features that contribute 90% to the final feature set sorting by importance in SBP. Therefore, we recommend using the 15 features if there are fewer

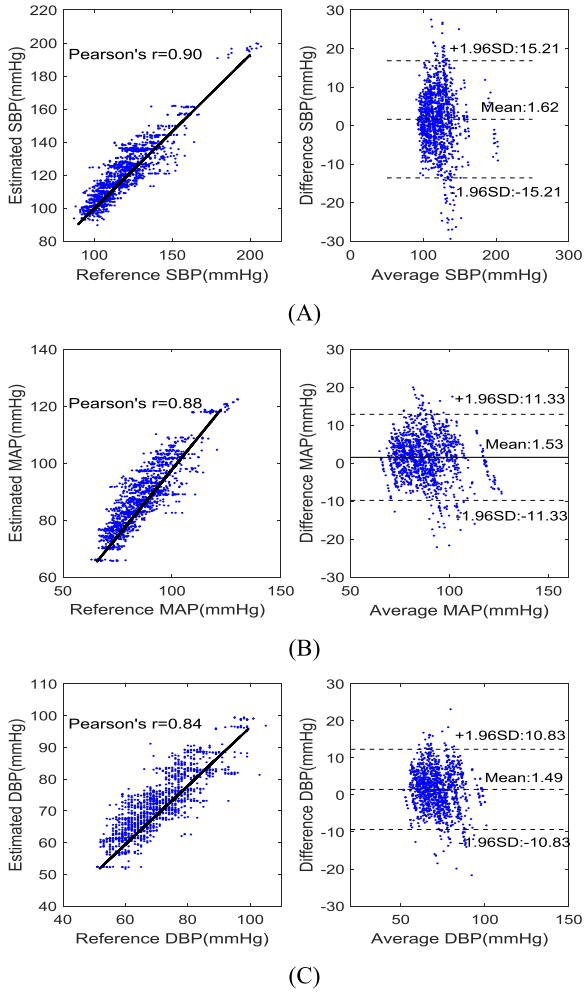


Fig. 12. Correlation and Bland–Altman plots of SBP, MAP, and DBP with reference cuff-based BP. (A) SBP estimation. (B) MAP estimation. (C) DBP estimation.

training data. The results confirm the importance of some previous reported physiological parameters including PTT, PIR, multiple features extracted from the 2nd PPW in BP estimation. Furthermore, informative parameters extracted from the time domain (SD, MN), frequency domain (Fre1, Fre3) and entropy properties (Approximate entropy) are also demonstrated with higher importance.

### *B. Accuracy Performance of the Proposed Models*

We evaluate the accuracy performance by average recordings for the whole population. Fig. 12 presents the overall correlation and Bland–Altman plot for the proposed SBP, MAP, and DBP estimations versus the reference cuff-based BP for all 85 participants. The correlation plot shows that the correlation coefficients for the SBP, MAP, and DBP estimates and the cuff-based measurements were 0.90, 0.88, and 0.84, respectively, which suggested a high correlation between the estimated BP and the reference. The Bland–Altman plot shows that most of the estimated points for SBP, MAP, and DBP were within $1.62 \pm 15.21$, $1.53 \pm 11.33$ and $1.49 \pm 10.83$ limits. Therefore, BP estimated

TABLE V
ACCURACY PERFORMANCE OF THE PROPOSED MODEL

| | Index | SBP | MAP | DBP |
|---|---|---|---|---|
| **AAMI** | ME(mmHg) | 1.62 | 1.53 | 1.49 |
| | STD(mmHg) | 7.76 | 6.03 | 5.52 |
| | AAMI | passed | passed | passed |
| **BHS** | C.P. 5 mmHg | 51% | 60% | 62% |
| | C.P. 10 mmHg | 81% | 90% | 92% |
| | C.P. 15 mmHg | 94% | 98% | 99% |
| | Grade | B | A | A |

(B) HYPERTENSIVE PATIENTS (17 SUBJECTS, 272 MEASUREMENTS)

| | Index | SBP | MAP | DBP |
|---|---|---|---|---|
| **AAMI** | ME(mmHg) | 2.03 | 1.82 | 1.73 |
| | STD(mmHg) | 7.68 | 6.01 | 5.43 |
| | AAMI | passed | passed | passed |
| **BHS** | C.P. 5 mmHg | 50% | 61% | 62% |
| | C.P. 10 mmHg | 82% | 89% | 91% |
| | C.P. 15 mmHg | 91% | 97% | 99% |
| | Grade | B | A | A |

C.P. 5 mmHg describes cumulative percentage of readings measured by the proposed approach are within ±5 mmHg of the reference cuff-based device.

by the proposed approach has the power to approximate BP measured using the cuff-based device.

Evaluation of the overall accuracy performance for both SBP and DBP estimation according to AAMI and BHS criteria is presented in Table V. Table V(A) and Table V(B) presents the performance for the overall 85 subjects and 17 hypertensive patients, respectively. The proposed method has an accuracy of $1.62 \pm 7.76$ mmHg for SBP estimation, $1.53 \pm 6.03$ mmHg for MAP estimation, and $1.49 \pm 5.52$ mmHg for DBP estimation in terms of ME $\pm$ STD, indicating that the proposed SBP, MAP and DBP model complies with AAMI criteria for the whole population, which require ME and STD values lower than 5 and 8 mmHg, respectively. Moreover, the SBP, MAP and DBP models comply with AAMI criteria for hypertensive patients, demonstrating the proposed method works properly in hypertensive population without taking antihypertensive drugs. According to the BHS standard, for both whole population and hypertensive population, the proposed method satisfies the requirements for grade A (CP at 5 mmHg $>$ 60%, CP at 10 mmHg $>$ 85%, and CP at 15 mmHg $>$ 95%) in MAP and DBP estimation while satisfying grade B (CP at 5 mmHg $>$ 50%, CP at 10 mmHg $>$ 75%, and CP at 15 mmHg $>$ 90%) in SBP estimation.

### C. Robustness Performance of the Proposed Models

Fig. 13 presents a day-by-day analysis of compliance to the BHS standard at D+1, D+3, D+6, D+8, and D+60 for SBP, MAP, and DBP estimation. A significant degradation of performance was observed from D+1 to D+3, but significant boosts were observed in performance from D+3 to D+6 and from D+8 and D+60. These results indicate that random daily fluctuation exists in the relationship between the proposed method and reference measurement, but it is not associated with long-term degradation. Therefore, such daily degradation might result from uncontrolled experimental conditions, such as measurement bias of the devices, rather than deterioration of the proposed approach. For example, the instructions for the sphygmomanometer used as the reference stated a ±3-mmHg bias for BP measurement.

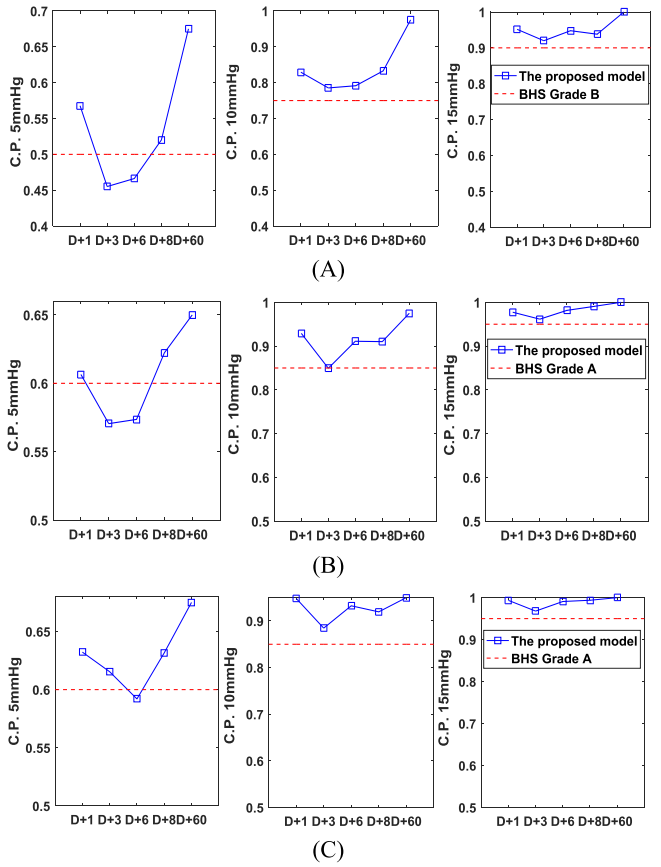


Fig. 13. Day-by-day evaluation of the performance according to BHS standard. (A) SBP estimation. (B) MAP estimation. (C) DBP estimation. C.P. 5 mmHg describes cumulative percentage of readings measured by the proposed approach are within ±5 mmHg of the reference cuff-based device.

### D. Computational Complexity of the Proposed Approach

The computational complexity of the proposed approach involved in three phases: the feature extraction, feature selection and the model development process. In the feature extraction process, the computational complexity depends on the number of channel $k$ used and the length of the each signal $l$ during one heartbeat. For feature extraction in one channel, the maximum computational complexity is $O(l\log(l))$ due to frequency transformation for each signal.

Thus the overall computational complexity is $O(k \times l\log(l))$. The computational complexity in the feature selection process depends on the number of data points $T$ in training dataset and the number of extracted features $M$ for selection. As the distance should be computed by each pairwise data points in training dataset, the computational complexity is $O(M^2 \times T^2)$. As multiple linear regression is used in model development process, the computational complexity also depends on the number of data points $T$ in training dataset due to solving normal equation. The optimized computational complexity is $O(T^2)$.

TABLE VI
PERFORMANCE COMPARISON WITH OTHER WORKS

| Work | Dataset | Follow-up period | Signals used | Calibration strategy | SBP | | | MAP | | | DBP | | |
|---|---|---|---|---|---|---|---|---|---|---|---|---|---|
| | | | | | ME (mmHg) | SD (mmHg) | MAE (mmHg) | ME (mmHg) | STD (mmHg) | MAE (mmHg) | ME (mmHg) | STD (mmHg) | MAE (mmHg) |
| **This work** | **85 aged participants** | **2m** | **ECG, 2-channel PPWs** | **Resting** | **1.62** | **7.76** | **6.13** | **1.53** | **6.03** | **4.81** | **1.49** | **5.52** | **4.54** |
| Multi-parameter [17], 2017 | 57 ICU patients in MIMIC III | - | ECG, PPG | Resting | - | - | 8.21 | - | - | - | - | - | 4.31 |
| Multi-parameter [19], 2017 | 73 healthy participants | 6m | ECG, PPG | Resting /Dynamic | -1.267 | 5.98 | - | - | - | - | -1.38 | 5.49 | - |
| Multi-parameter [18], 2017 | 23 ICU patients in MIMIC III | 1d | ECG, PPG | Resting | - | - | 8.7 | - | - | 5.6 | - | - | 4.4 |
| PTT&PIR[14], 2016 | 27 healthy participants | 1.5h | ECG, PPG | Resting | -0.37 | 5.21 | 4.09 | -0.08 | 4.06 | 3.18 | -0.18 | 4.13 | 3.18 |
| I-PTT [8], 2013 | 15 healthy male participants | 14d | ICG, ECG, PPG | Dynamic | - | - | - | -0.8 | 5.1 | - | - | - | - |

Commonly speaking, $k$, $l$ and $M$ are far less than $T$, thus the overall computational complexity can be denoted as $O(T^2)$.

### E. Comparison With Other Works

We compared the proposed approach with other works including multi-parameter and PTT based methods for BP estimation, as presented in Table VI. From Table VI, the number of participants in our study was considerably higher than in other works and involved diverse populations (17 hypertensive patients, 56 healthy participants, and 12 hypotensive patients) accompanied by a long-term follow-up period, suggesting the proposed approach has high reliability. Despite the performance of the proposed approach being below that in some studies examining young healthy populations [14], [19], it greatly outperformed work aimed at ICU patients [17], [18]. Moreover, existing studies for ICU patients were based on public MIMICII database, which is not designed specifically for BP estimation in routine life but only record information in the ICU cohort and with a low sample rate (150 Hz for ECG and PPG signal). Although 3-channel signals are used in our study, the increase on the overall computational complexity is acceptable from the analysis in Section V.D. Therefore, the proposed work is with high accuracy and reliability performance with an elaborately designed experimental protocol.

## VI. DISCUSSION

This study examined a novel concept for BP estimation using a multi-sensor fusion method. Different measures of PTT were employed in the proposed method, with an emphasis on the combination of information from PPW signals.

### A. Evaluation of Different Measures of PTT in BP Estimation

PTT has recently been studied for use in cuff-less BP estimation; however, the most effective method for measuring PTT remains controversial. The most commonly used PTT is calculated as the time delay from ECG R-wave to the pulse wave (i.e., PPG). This measurement can easily be implemented in a wearable device, and several studies have demonstrated

TABLE VII
PERFORMANCE EVALUATION OF THREE MEASURES OF PTT

| | SBP | | | DBP | | |
|---|---|---|---|---|---|---|
| | PTTeb | **PTTea** | PTTba | PTTeb | **PTTea** | PTTba |
| **Overall accuracy** | 1.68±8.51 | **1.34±8.09** | 1.43±9.13 | 1.72±5.88 | **1.41±5.66** | 1.51±6.04 |
| **Accuracy on D+1** | 0.72±8.40 | **0.82±8.05** | 0.94±8.45 | 0.72±5.88 | **0.71±5.84** | 0.93±6.01 |
| **Accuracy on D+3** | 1.71±9.16 | **1.96±8.61** | 2.44±8.85 | 2.07±6.21 | **1.76±5.94** | 1.89±6.18 |
| **Accuracy on D+6** | 1.57±8.78 | **0.75±8.01** | 0.65±9.94 | 1.93±6.14 | **1.43±5.65** | 1.56±6.12 |
| **Accuracy on D+8** | 2.53±7.68 | **1.42±7.56** | 1.57±9.44 | 2.45±5.22 | **1.96±5.27** | 2.00±5.81 |
| **Accuracy on D+60** | -0.97±9.02 | **-2.02±7.24** | 1.79±8.02 | 2.06±5.97 | **0.63±5.41** | 1.69±5.44 |

that PTT with PEP included has a positive effect on BP estimation [42]. However, several researchers have found that PTT calculated from two PPG sensors or ICG to PPG has greater correlation with BP [12], [53]. Therefore, to better and fairly compare the performance of different measures of PTT in BP estimation with the same dataset, two channels of PPW signals were selected in this study to compute three PTTs —PTTeb, PTTea, and PTTba combined with ECG signal.

This study evaluated three measures of PTT—PTTeb, PTTea, and PTTba—for BP estimation during daily activities among middle-aged or elderly populations. Table VI presents the performance comparison of estimation accuracy at different calibration interval among the three models developed based on each PTT. From Table VII, PTTea had the best estimation accuracy at different intervals after calibration for both SBP and DBP. This finding supports the results in that the inclusion of PEP led to greater estimation accuracy. However, during the two measures of PTT that included PEP, PTTea was more stable because of the longer transmission distance and thus could better describe the entire circulation system of human body.

The estimation accuracy comparison at different intervals showed similar patterns of robustness between PTTea and PTTba; that is, the performance fluctuated to a certain degree for different time intervals. Nevertheless, long-term degrada-

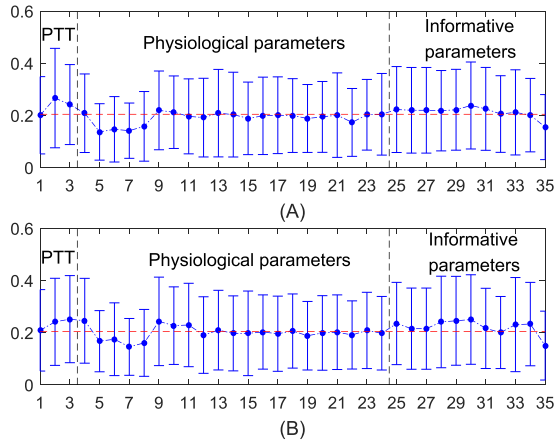


Fig. 14. Mean ± SD of the correlation coefficients for the extracted physiological parameters and informative features for SBP and DBP. (A) Correlation coefficient for each feature with SBP. (B) Correlation coefficient for each feature with DBP.

tion was observed for PTTeb (from 2.53 ± 7.68 at day D+8 to −0.97 ± 9.02 at day D+60), explaining why frequent calibration was needed to ensure the estimation performance for PTTeb-based methods [18].

### B. Performance Evaluation of PPW Signals in BP Estimation

Although various studies have demonstrated the feasibility of PPG signals in improving PTT-based BP estimation [16], few studies have been conducted on the verification of PPW signals, which are an intuitive representation of the arterial BP waveform with more redundant information than PPG signals provide, in BP estimation. In our previous work, we presented a critical evaluation of the PPW in BP estimation based on the feature points in PPW signals, and the results showed that the PPW is a potential method for BP estimation [49]. In the present study, in addition to the physiological parameters extracted based on feature points, informative parameters extracted based on signal property were evaluated for BP estimation. Fig. 14 shows that compared with physiological parameters, informative parameters had slightly greater correlation with BP. Informative parameters have stable properties, and thus there is no need to extract feature points, which are highly influenced by signal quality. Therefore, informative parameters from the PPW are favorable choices for BP estimation. PPW signals are normally inconvenient to record; however, with the advanced development of electric fabrics and flexible pressure sensors, the PPW can be stably collected through a wearable device comprising a flexible pressure sensor array attached to the skin to collect multipoint pressure waveforms during daily activities and home-care monitoring [26], [27]. Therefore, PPW is with great potential for improving the performance of cuff-less BP estimation.

### C. Limitations

We finalize the discussion by presenting the limitations of this study. First, recordings were collected in a controlled scenario with participants required to lie down quietly to avoid movement artifacts. The sitting posture is allowed in practical application. Second, the current configuration of the sensors for collecting signals restricted its application in un-obstructive BP measurements; however, we believe that the sensors can be reconfigured in a portable manner with the development of flexible pressure sensor arrays.

## VII. Conclusions and Future Work

This paper proposed a multi-sensor fusion based approach for cuff-less BP estimation with high reliability and robustness, which is comprised of one-channel ECG and two-channel PPW sensors. Physiological and informative parameters were extracted from three-channel signals, and a WSF selection method based on spectral analysis was proposed to obtain the most promising indicators for each subject. A multi-instance regression method was employed to develop the BP model. The performance of the proposed approach was validated on 85 middle-aged or elderly participants (including 17 hypertensive patients, 56 healthy subjects and 11 hypotensive patients). Experimental results showed that the proposed approach complied with the AMMI standards in SBP, MAP and DBP estimation for diverse population. Moreover, compared with PTT and multi-parameter based methods, the proposed models achieves better robustness through a maximum of 2-month follow-up period. Overall, this paper provides a high reliable and robust method for cuff-less BP measurement.

Future work will focus on a wearable system that apply an advanced flexible pressure sensor array to provide a cuff-less BP model in wearable manner. Moreover, a universal and simplified calibration strategy should be studied to facilitate widespread adoption.

## References

[1] *World Health Statistic*. Geneva, Switzerland: World Health Organization, 2015.
[2] D. T. Lackland and M. A. Weber, "Global burden of cardiovascular disease and stroke: Hypertension at the core," *Can. J. Cardiology*, vol. 31, no. 5, pp. 569–571, May 2015.
[3] World Health Organization, "A global brief on hypertension: Silent killer, global public health crisis: World Health Day 2013," 2013.
[4] J. Lu *et al.*, "Prevalence, awareness, treatment, and control of hypertension in China: data from 1Â·7 million adults in a population-based screening study (China PEACE million persons project)," *Lancet*, vol. 390, no. 10112, pp. 2549–2558, 2017.
[5] Y. T. Zhang, Y. L. Zheng, W. H. Lin, H. Y. Zhang, and X. L. Zhou, "Challenges and opportunities in cardiovascular health informatics," *IEEE Trans. Biomed. Eng.*, vol. 60, no. 3, pp. 633–642, Mar. 2013.
[6] A. Chandrasekhar *et al.*, "Smartphone-based blood pressure monitoring via the oscillometric finger-pressing method," *Sci. Translational Med.*, vol. 10, no. 431, 2018, Art. no. eaap8674.
[7] A. Chandrasekhar *et al.*, "An iPhone application for blood pressure monitoring via the oscillometric finger pressing method," *Sci. Rep.*, vol. 8, no. 1, 2018, Art. no. 13136.
[8] M. A. Zakrzewski, A. Y. Huang, R. Zubajlo, and B. W. Anthony, "Real-time blood pressure estimation from force-measured ultrasound," *IEEE Trans. Biomed. Eng.*, vol. 65, no. 11, pp. 2405–2416, Nov. 2018.
[9] P. M. Nabeel, J. Joseph, S. Karthik, M. Sivaprakasam, and M. Chenniappan, "Bi-modal arterial compliance probe for calibration-free cuffless blood pressure estimation," *IEEE Trans. Biomed. Eng.*, vol. 65, no. 11, pp. 2392–2404, Nov. 2018.

[10] X. R. Ding *et al.*, "Continuous blood pressure measurement from invasive to unobtrusive: Celebration of 200th birth anniversary of Carl Ludwig," *IEEE J. Biomed. Health Inform.*, vol. 20, no. 6, pp. 1455–1465, Nov. 2016.

[11] R. Mukkamala *et al.*, "Toward ubiquitous blood pressure monitoring via pulse transit time: Theory and practice," *IEEE Trans. Biomed. Eng.*, vol. 62, no. 8, pp. 1879–1901, Aug. 2015.

[12] J. Solà *et al.*, "Noninvasive and nonocclusive blood pressure estimation via a chest sensor," *IEEE Trans. Biomed. Eng.*, vol. 60, no. 12, pp. 3505–3513, Dec. 2013.

[13] T. H. Huynh, R. Jafari, and W. Chung, "Noninvasive cuffless blood pressure estimation using pulse transit time and impedance plethysmography," *IEEE Trans. Biomed. Eng.*, vol. 66, no. 4, pp. 967–976, Apr. 2019. doi: 10.1109/TBME.2018.2865751.

[14] C. C. Y. Poon and Y. T. Zhang, "Cuff-less and noninvasive measurements of arterial blood pressure by pulse transit time," in *Proc. 27th Annu. Conf. IEEE Eng. Med. Biol.*, Shanghai, China, 2005, pp. 5877–5880.

[15] Q. Liu, B. P. Yan, C. M. Yu, Y. T. Zhang, and C. C. Y. Poon, "Attenuation of systolic blood pressure and pulse transit time hysteresis during exercise and recovery in cardiovascular patients," *IEEE Trans. Biomed. Eng.*, vol. 61, no. 2, pp. 346–352, Feb. 2014.

[16] Y. L. Zheng, B. P. Yan, Y. T. Zhang, and C. C. Y. Poon, "An armband wearable device for overnight and cuff-less blood pressure measurement," *IEEE Trans. Biomed. Eng.*, vol. 61, no. 7, pp. 2179–2186, Jul. 2014.

[17] X. R. Ding, Y. T. Zhang, J. Liu, W. X. Dai, and H. K. Tsang, "Continuous cuffless blood pressure estimation using pulse transit time and photoplethysmogram intensity ratio," *IEEE Trans. Biomed. Eng.*, vol. 63, no. 5, pp. 964–972, May 2016.

[18] X. R. Ding, Y. T. Zhang, and H. K. Tsang, "Impact of heart disease and calibration interval on accuracy of pulse transit time-based blood pressure estimation," *Physiological Meas.*, vol. 37, no. 2, pp. 227–237, 2016.

[19] W. H. Lin, H. Wang, O. W. Samuel, G. Liu, Z. Huang, and G. L. Li, "New photoplethysmogram indicators for improving cuffless and continuous blood pressure estimation accuracy," *Physiological Meas.*, vol. 39, no. 2, Fed. 2018, Art. no. 025005.

[20] M. Kachuee, M. M. Kiani, H. Mohammadzade, and M. Shabany, "Cuffless blood pressure estimation algorithms for continuous health-care monitoring," *IEEE Trans. Biomed. Eng.*, vol. 64, no. 4, pp. 859–869, Apr. 2017.

[21] Y. Z. Yoon *et al.*, "Cuff-less blood pressure estimation using pulse waveform analysis and pulse arrival time," *IEEE J. Biomed. Health Inform.*, vol. 22, no. 4, pp. 1068–1074, Jul. 2018.

[22] F. Miao *et al.*, "A novel continuous blood pressure estimation approach based on data mining techniques," *IEEE J. Biomed. Health Inform.*, vol. 21, no. 6, pp. 1730–1740, Nov. 2017.

[23] X. He, R. A. Goubran, and X. P. Liu, "Secondary peak detection of PPG signal for continuous cuffless arterial blood pressure measurement," *IEEE Trans. Instrum. Meas.*, vol. 63, no. 6, pp. 1431–1439, Jun. 2014.

[24] R. He, Z. P. Huang, L. Y. Ji, and J. K. Wu, "Beat-to-beat ambulatory blood pressure estimation based on random forest," in *Proc. IEEE Int. Conf. Wearable Implantable Body Sens. Netw.*, 2016, pp. 194–198.

[25] Z. Xu, J. Liu, X. Chen, Y. Wang, and Z. Zhao, "Continuous blood pressure estimation based on multiple parameters from eletrocardiogram and photoplethysmogram by back-propagation neural network," *Comput. Ind.*, vol. 89, pp. 50–59, 2017.

[26] D. D. He, E. S. Winokur, and C. G. Sodini, "An ear-worn vital signs monitor," *IEEE Trans. Biomed. Eng.*, vol. 62, no. 11, pp. 2547–2552, Nov. 2015.

[27] J. Allen, "Photoplethysmography and its application in clinical physiological measurement," *Physiological Meas.*, vol. 28, no. 3, 2007, Art. no. R1.

[28] A. Bhagat, N. Kapoor, and H. Bhagat, "Pulse wave analysis as an experimental tool to clinical application: Past and present (review)," *Acta Physiologica Hungarica*, vol. 98, no. 4, pp. 382–392, 2011.

[29] J. P. Lekakis, N. A. Zakopoulos, A. D. Protogerou, T. G. Papaioannou, V. T. Kotsis, and P. Vch, "Arterial stiffness assessed by pulse wave analysis in essential hypertension: Relation to 24-h blood pressure profile," *Int. J. Cardiology*, vol. 102, no. 3, pp. 391–395, 2005.

[30] Y. Pang *et al.*, "Flexible, highly sensitive and wearable pressure and strain sensors with graphene porous network structure," *ACS Appl. Mater. Interfaces*, vol. 8, no. 40, pp. 26458–26462, 2016.

[31] Z. Chen *et al.*, "Flexible piezoelectric-induced pressure sensors for static measurements based on nanowires/graphene heterostructures," *ACS Nano*, vol. 11, no. 5, pp. 4507–4513, 2017.

[32] F. Affecting, "Factors that affect blood pressure," 1997. [Online]. Available: http://www.siaweb.dk/af/misc/assignmentfiles/cardiovascular/Fact_Aff_Blood_Pressure.pdf

[33] I. S. Mackenzie, I. B. Wilkinson, and J. R. Cockcroft, "Assessment of arterial stiffness in clinical practice," *QJM Monthly J. Assoc. Physicians*, vol. 95, no. 2, pp. 67–74, 2002.

[34] M. F. O'Rourke, A. Pauca, and X. J. Jiang, "Pulse wave analysis," *Brit. J. Clin. Pharmacology*, vol. 51, no. 6, pp. 507–522, 2001.

[35] Z. Fan, G. Zhang, and S. Liao, "Pulse wave analysis," in *Advanced Biomedical Engineering*. Rijeka, Croatia: InTech, 2011.

[36] R. Liang and Q.-M. Wang, "Pulse pressure sensor based on flexible PZT thick-film composite device," in *Proc. IEEE Int. Ultrason. Symp.*, Chicago, IL, USA, 2014, pp. 1559–1562.

[37] S. Hansen and M. Staber, "Oscillometric blood pressure measurement used for calibration of the arterial tonometry method contributes significantly to error," *Eur. J. Anaesthesiology*, vol. 23, no. 9, pp. 781–787, 2016.

[38] D. J. Hughes *et al.*, "Measurements of Young's modulus of elasticity of the canine aorta with ultrasound," *Ultrason. Imag.*, vol. 1, no. 1, pp. 356–367, 1979.

[39] N. Westerhof *et al.*, "The arterial windkessel," *Med. Biol. Eng. Comput.*, vol. 47, pp. 131–141, 2009.

[40] M. Butlin, F. Shirbani, E. Barin, I. Tan, B. Spronck, and A. Avolio, "Cuffless estimation of blood pressure: Importance of variability in blood pressure dependence of arterial stiffness across individuals and measurement sites," *IEEE Trans. Biomed. Eng.*, vol. 65, no. 11, pp. 2377–2383, Nov. 2018.

[41] R. A. Payne *et al.*, "Pulse transit time measured from the ECG: An unreliable marker of beat-to-beat blood pressure," *J. Appl. Physiol.*, vol. 100, no. 1, pp. 136–141, 2000.

[42] M. Y. Wong *et al.*, "The effects of pre-ejection period on post-exercise systolic blood pressure estimation using the pulse arrival time technique," *Eur. J. Appl. Physiol.*, vol. 111, no. 1, pp. 135–144, 2011.

[43] Z. D. Liu *et al.*, "Cuffless blood pressure estimation using pressure pulse wave signals," *Sensors*, vol. 18, no. 12, 2018, Art. no. 4227.

[44] S. M. Pincus, I. M. Gladstone, and R. A. Ehrenkranz, "A regularity statistic for medical data analysis," *J. Clin. Monit.*, vol. 7, no. 4, pp. 335–345, 1991.

[45] Y. Zheng *et al.*, "Predicting arterial stiffness from radial pulse waveform using support vector machines," *Procedia Eng.*, vol. 7, no. 7, pp. 458–462, 2010.

[46] Z.-H. Zhou, "A brief introduction to weakly supervised learning," *Nat. Sci. Rev.*, vol. 5, pp. 44–53, 2018.

[47] Z. Li, Y. Yang, J. Liu, X. Zhou, and H. Lu, "Unsupervised feature selection using nonnegative spectral analysis," in *Proc. AAAI Conf. Artif. Intell.*, 2012, vol. 2, pp. 1026–1032.

[48] Z. Zheng and H. Liu, "Spectral feature selection for supervised and unsupervised learning," in *Proc. 24th Int. Conf. Mach. Learn.*, 2007, pp. 1151–1157.

[49] E. O. Brien *et al.*, "The British hypertension society protocol for the evaluation of automated and semi-automated blood pressure measuring devices with special reference to ambulatory systems," *J. Hypertension*, vol. 8, no. 7, pp. 607–619, 1990.

[50] *American National Standard for Electronic or Automated Sphygmomanometers*, ANSI/AAMI SP 10 2002, Arlington, VA, USA: Association for the Advancement Instrumentation, 2002.

[51] M. Robnik-Šikonja and I. Kononenko, "Theoretical and empirical analysis of ReliefF and RReliefF," *Mach. Learn.*, vol. 53, no. 1-2, pp. 23–69, 2003.

[52] D. Cai, C. Zhang, and X. He, "Unsupervised feature selection for multi-cluster data," in *Proc. 16th ACM SIGKDD Int. Conf. Knowl. Discovery Data Mining*, Jul. 2010, pp. 333–342.

[53] M. Gao, N. B. Olivier, and R. Mukkamala, "Comparison of noninvasive pulse transit time estimates as markers of blood pressure using invasive pulse transit time measurements as a reference," *Physiological Rep.*, vol. 4, no. 10, 2016, Art. no. e12768.